Research Article | Vol. 28, No. 16 / 3 August 2020 / Optics Express 23060

Optics EXPRESS

Multi-pitch self-calibration measurement using a nano-accuracy surface profiler for X-ray mirror metrology

LEI HUANG,[1,*] TIANYI WANG,[1] JOSEP NICOLAS,[2] FRANÇOIS POLACK,[3] CHAO ZUO,[4] KASHMIRA NAKHODA,[1] AND MOURAD IDIR[1]

[1]National Synchrotron Light Source II, Brookhaven National Laboratory, Upton, NY 11973, USA
[2]ALBA Synchrotron Light Source, Carrer de la Llum 2-26, 08290, Cerdanyola del Vallès, Spain
[3]Synchrotron SOLEIL, L'Orme des Merisiers, Saint-Aubin, BP 48, 91192 Gif-sur-Yvette Cedex, France
[4]School of Electronic and Optical Engineering, Nanjing University of Science and Technology, No. 200 Xiaolingwei Street, Nanjing, Jiangsu Province 210094, China
[*]huanglei0114@gmail.com

Abstract: For high accuracy X-ray mirror measurement, the analysis and corrections of minute systematic errors of the measuring instrument are required. As an X-ray mirror metrology tool, the nano-accuracy surface profiler (NSP) consists of two autocollimators (AC) serving its reference and sample beams, in which the sample-beam AC maintains a fixed distance from the mirror. In this work, the multi-pitch self-calibration method is applied to an NSP instrument to reconstruct both the mirror slope and the instrument error of the sample-beam AC through a series of x scans and pitch angle scans. It is more technically sound to apply this multi-pitch self-calibration method to a working-distance-fixed slope scanner, such as the NSP. First of all, we introduce the principle of the multi-pitch self-calibration method, discuss its ambiguities, and provide our regularization illustrated with simulations. Second, some real measurements of a spherical mirror with 10-mrad total slope are demonstrated to verify the effectiveness of the multi-pitch self-calibration technique with an NSP. Furthermore, the experimental reconstruction of the low- and high-frequency signals of the instrument error with different settings in x and pitch steps are addressed and studied in terms of repeatability, reproducibility, self-consistency, and effectiveness in compensation for single-pitch scans.

1. Introduction

With the technical improvement of the diffraction-limited storage ring and free-electron lasers, the produced X-ray beam quality is getting higher. Correspondingly, to perfectly transport or focus the X-ray beam at the diffraction limit, the requirement on the X-ray optics becomes tighter. The figure error of X-ray mirrors is typically getting down to sub-100 nrad RMS in slope or sub-nm RMS in height to preserve the high quality of the beams [1].

At many synchrotron radiation facilities, like NSLS-II, X-ray mirrors are generally inspected with the point-wise scanning deflectometric profilers [2–13]. These metrology tools have been developed in the late 1980s from the Long Trace Profiler (LTP) by Takacs *et al.* [2], to the autocollimator (AC) based Nanometer Optical component measuring Machine (NOM) by Siewert *et al.* in 2004 [6]. These two options have been widely implemented in the synchrotron facilities around the world [7,9,10]. With some improvements, the Nano-accuracy Surface Profiler (NSP) was recently developed by Qian *et al.* [11]. As the metrology requirement is getting stricter, the intrinsic instrument error of the optical head or the AC needs to be characterized and calibrated by a more accurate small angle generator to further improve the measurement accuracy [12,14–16].

#392433 https://doi.org/10.1364/OE.392433
Journal © 2020 Received 10 Mar 2020; revised 15 May 2020; accepted 1 Jun 2020; published 20 Jul 2020

Optics EXPRESS

Since the proposal [17] and the suggestion [3] of using a moving pentaprism, the pentaprism-based LTP/NOM has become the dominant system in X-ray mirror metrology [4,6,8,10]. Using this geometry to measure an X-ray mirror surface as the Surface Under Test (SUT), the Sensor-to-SUT Distance (SSD) changes during the pentaprism motion. Because the instrument error is distance dependent [14,18,19], it is not technically sound to apply a distance-fixed calibration to such an SSD-varying scan. On the other hand, the SSD is fixed in the NSP principle, typically between 5 mm to 10 mm. This very short distance brings practical difficulties in the AC calibration. One way to overcome this issue was proposed by Lacey *et al.* to transfer the calibration from one calibrated reference AC to the scanning AC mounted on the gantry [16].

Another way to compensate the instrument error was proposed by Polack *et al.* while they were developing an LTP stitching procedure with the estimation of the instrument error [20,21]. Nicolas *et al.* applied a similar instrument error suppression algorithm in the calibration of mechanical mirror benders [22] and the continuous scanning ALBA-NOM [23]. When applying this instrument error suppression algorithm with multi-pitch redundant angular dataset to a moving-pentaprism-based LTP/NOM system, it is assumed that the instrument error is the same in all scans with different pitches.

However, due to the distance dependency of the instrument error [14,18,19], this assumption may not be always "true" in a moving-pentaprism-based LTP/NOM case, especially when the

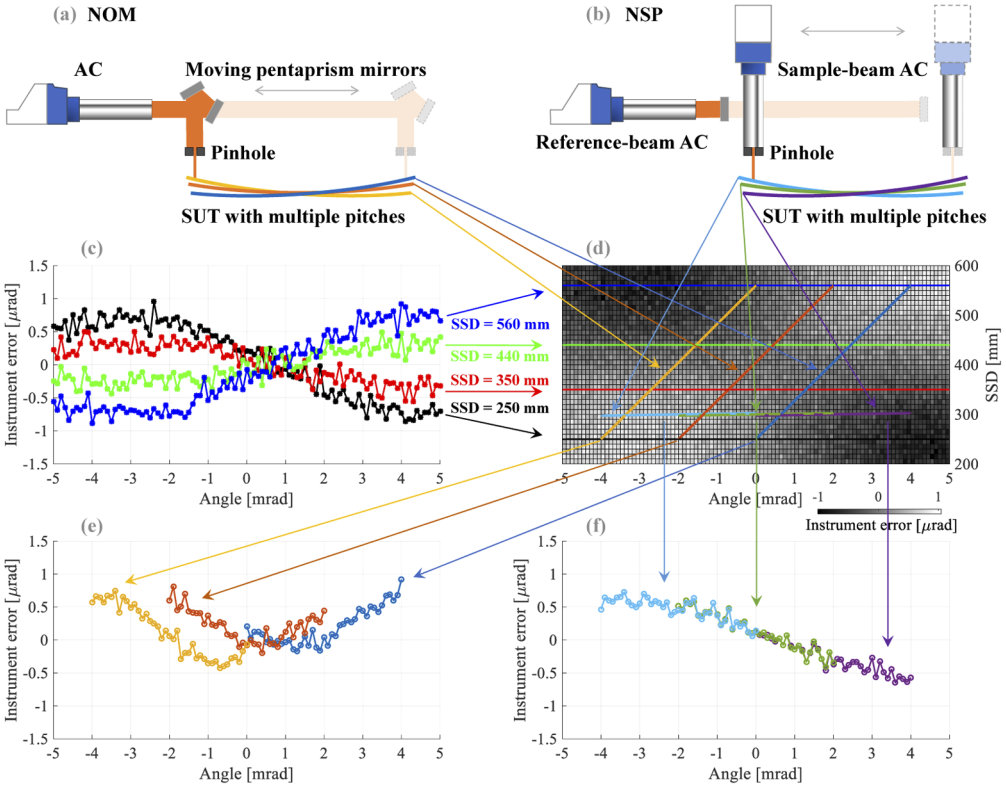

Fig. 1. Due to the distance dependency of the instrument error, the NSP is more suitable than the LTP/NOM to implement the multi-pitch measurement. Sketches of NOM (a) and NSP (b) in a multi-pitch measurement scheme, (c) the simulated instrument error curves at different distances referring to Fig. 4(b) in Ref. [14], (d) the simulated 2D instrument error as a function of the angle and the SSD, (e) the instrument error *vs* the angle for a varying-SSD system, and (f) the instrument error *vs* the angle for a fixed-SSD system.

Optics EXPRESS

pitch range is large. This is illustrated in Fig. 1. A 2D instrument error map is simulated as a function of the angle $\alpha \in [-5, 5]$ mrad and the SSD $\in [200, 600]$ mm in Fig. 1(d). On this error map whose amplitude is $\pm 1\mu$rad, the measurement paths for NSP and LTP/NOM are superimposed. The instrument error curves in Fig. 1(c) at distances SSDs = 250 mm, 350 mm, 440 mm, and 560 mm is simulated referring to the Fig. 4(b) in Ref. [14]. Figure 1(e) displays the instrument error curves of a moving-pentaprism-based LTP/NOM in multi-pitch measurement have large discrepancies in the overlapping angular ranges with a 2 mrad pitch step and 310 mm varying working distance. As a contrast, the instrument error curves of an NSP in multi-pitch measurement coincide well with a 2 mrad pitch step and 5 mm distance variations as shown in Fig. 1(f). Since the SSD of the sample-beam AC in NSP is fixed as illustrated in Figs. 1(b), the instrument error can reasonably be assumed the same in all scans with different pitches. For instance, with an $L = 1$ m long mirror and $R_p = 10$ mrad active pitch range, if NSP SSD = 300 mm (In real measurement, the NSP SSD should be around 10 mm. Here we have simulated instrument error map with SSD from 200 mm to 600 mm only, so we assume NSP SSD is fixed as 300 mm for illustration purpose.), the SSD only changes $L/2 \cdot R_p = 5$ mm, and as illustrated in Figs. 1(d) and 1(f), the instrument error curves are very close to each other with 5 mm distance variation. It indicates that the NSP is an ideal instrument to employ the multi-pitch instrument error reduction algorithm. Therefore, in this work, we apply the multi-pitch method to the NSP to improve the measurement accuracy by estimating the instrument error from the redundant angular dataset with the linear least squares method. In addition, the ambiguities in the multi-pitch algorithm are addressed by applying corresponding constraints to the pitch angle and instrument error function. The feedback from an extra pitch-beam AC is compared with the estimated pitch angles. Moreover, to get a smaller matrix condition number in the linear least squares estimation, parametric settings are discussed to keep the result being less sensitive to the measurement noise.

2. Principle of multi-pitch self-calibration measurement with NSP

The multi-pitch NSP measurement system layout is shown in Fig. 2. Three ACs are used to measure the angles of interest. The 15-mm-aperture reference-beam AC couples with a flat mirror to track the pitch angle of the carriage, on which the sample-beam AC scans the SUT through a 2.5-mm-diameter pinhole. The 50-mm-aperture pitch-beam AC coupled with another flat mirror measures the pitch angle of the pitch stage which holds the sample mirror.

With a commercially available air-bearing stage, the pitch error can remain below 10 μrad during 1-m-long motion. The pitch-beam AC, which is optional, provides assistant information of the active pitch angles. The x and pitch motions as well as the angle and temperature data acquisition are controlled by a home developed software written in C++ and Qt. The instrument error of the sample-beam AC is estimated by using the multi-pitch algorithm described in the following section.

2.1. Mathematical model and optimization

With the nth active pitch angle θ_n in total N pitches $\boldsymbol{\theta} = [\theta_1, \theta_2, \ldots, \theta_N]$, combining the measured angles at NSP coordinates x from the sample-beam AC, $m_n(x)$, and the reference-beam AC, $r_n(x)$, the local surface tilt measurement $m_n(x) + r_n(x)$ (the sign depends on actual AC orientations, and here the sign is "+" in our NSLS-II NSP setup) can be described by the expression

$$m_n(x) + r_n(x) = s(x^s) + e(m_n(x)) + \theta_n + n_a, \quad n \in [1, N], \tag{1}$$

where $s(x^s)$ is the mirror surface slope at SUT coordinates x^s, the term $e(m_n(x))$ stands for the instrument error of the sample-beam AC while its angular reading is $m_n(x)$, the angle θ_n is the nth actively introduced pitch, and n_a represents uncorrelated additive random noise. The pupil of the reference-beam AC is sufficiently large, so the noise of r_n is much smaller than the one in m_n

Optics EXPRESS

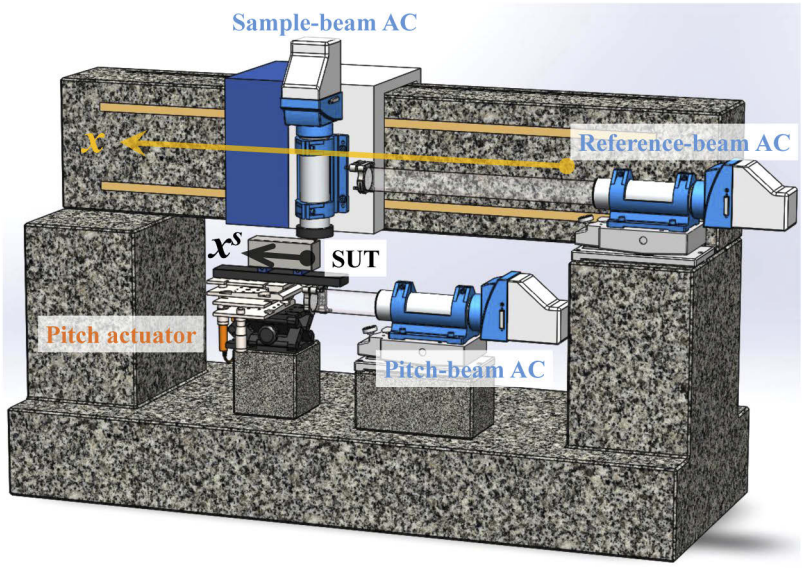

Fig. 2. The layout of the multi-pitch self-calibration NSP. The reference-beam AC coupled with a flat mirror measures the pitch angle of an air-bearing carriage. The SUT placed on the sample stage is scanned by the sample-beam AC moving along the carriage. The pitch angle of the sample stage can be actively adjusted, and a pitch-beam AC coupled with a flat mirror can monitor the pitch angle of the sample stage.

and there are much less diffraction effects that cause periodic errors by pixel interpolation. More importantly, the reference-beam AC always measures angles near zero within few microradians, so the retrace errors are minimal and negligible.

In the real experiment, the center of rotation of the active pitch stage is usually not in the plane of the mirror surface. This can introduce a pitch-dependent horizontal shift between the actual sampling locations x_n^s in SUT coordinates and the NSP stepping position x in NSP coordinates which is consistent for all pitch angles. By applying the rotation relation, we have

$$x_n^s = x \cdot \cos(-\theta_n) - d \cdot \sin(-\theta_n) = x \cdot \cos\theta_n + d \cdot \sin\theta_n \approx x + d \cdot \theta_n, \tag{2}$$

where d is the distance between the center of rotation of the pitch stage and the mirror surface.

Two independent uniform cubic B-splines $\boldsymbol{B}(\boldsymbol{x^s})$ and $\boldsymbol{E}(\boldsymbol{m})$, where $\boldsymbol{x^s} = [\boldsymbol{x_1^s}, \boldsymbol{x_2^s}, \ldots, \boldsymbol{x_N^s}]$ and $\boldsymbol{m} = [\boldsymbol{m_1}, \boldsymbol{m_2}, \ldots, \boldsymbol{m_N}]$, are used to represent two unknown functions, the SUT slope $s(\boldsymbol{x^s}) = \boldsymbol{B}(\boldsymbol{x^s})\boldsymbol{c}^\top$ and the instrument error $e(\boldsymbol{m}) = \boldsymbol{E}(\boldsymbol{m})\boldsymbol{f}^\top$. The problem is converted to estimate the unknown coefficient vectors $\boldsymbol{c}$ and $\boldsymbol{f}$. Therefore, Eq. (1) becomes

$$\begin{aligned} m_n(x) + r_n(x) &\approx s(x + d \cdot \theta_n) + e(m_n(x)) + \theta_n + n_a \\ &= \boldsymbol{B}(x + d \cdot \theta_n)\boldsymbol{c}^\top + \boldsymbol{E}(m_n(x))\boldsymbol{f}^\top + \theta_n + n_a, \quad n \in [1, N]. \end{aligned} \tag{3}$$

In this equation, the stepping position in NSP coordinates x, the sample-beam reading $m_n(x)$, the reference-beam reading $r_n(x)$, and the distance between SUT and pitch rotation axis d are known in our measurement. Therefore, the basis of B-splines $\boldsymbol{B}(x + d \cdot \theta_n)$ and $\boldsymbol{E}(m_n(x))$ are known as well. During the optimization process, we need to find the best coefficients $\boldsymbol{c}$ and $\boldsymbol{f}$ as well as the pitch angles $\boldsymbol{\theta}$ that best explain the measured data in a least square sense as described with the follow expression.

$$\min_{\boldsymbol{c},\boldsymbol{f},\boldsymbol{\theta}} \sum_{n=1}^{N} \sum_{x} \left(m_n(x) + r_n(x) - \boldsymbol{B}(x + d \cdot \theta_n)\boldsymbol{c}^\top - \boldsymbol{E}(m_n(x))\boldsymbol{f}^\top - \theta_n \right)^2 \tag{4}$$

Optics EXPRESS

Before minimizing the residuals, the ambiguities among solutions need to be addressed. Some proper regularization is necessary to avoid the measurement data to be well explained with different $\boldsymbol{c}, \boldsymbol{f}$ and $\boldsymbol{\theta}$.

2.2. Ambiguities and regularization

The angular bias ambiguity. It is not difficult to find that the bias values of the SUT slope, instrument error, and active pitch are coupled together with their sum equaling to the bias value of $m_n(x)$. In order to get rid of this ambiguity, we need to regularize two of these three angular bias values. This can be done by defining the origins of the angles.

First, we define the first pitch angle $\theta_1 = 0$ for simplicity. It is also a natural choice for the slope stitching process, as we can let the stitching start from the sample-beam AC reading at the left end of the SUT close to 0, and after all the pitch scans, the sample-beam AC reading at the right end of the SUT coming back to 0 to make sure the stitching covers the whole space and slope ranges with redundancy.

Second, it is preferable to define the instrument error as 0 while its reading is 0, *i.e.* $e(0) = 0$ as implemented as $\boldsymbol{E}(0)\boldsymbol{f}^\top = 0$. It is equivalent to that the sample-beam AC and the calibration tool are well aligned with both readings are 0 during an AC calibration.

In this case, the resultant SUT slope offset will be fixed to a unique solution with $e(0) = 0$ and $\theta_1 = 0$. Since the slope offset is actually a tilt in height which is not of interest for X-ray mirror surface shape measurement, the above regularization is acceptable.

The angular linear term ambiguity. If we consider to separate the instrument error $e(m) = \varepsilon \cdot m + e_h(m)$ as its linear term $\varepsilon \cdot m$ and other higher orders $e_h(m)$, Eq. (3) becomes

$$m_n(x) + r_n(x) = s(x^s) + \varepsilon \cdot m_n(x) + e_h(m_n(x)) + \theta_n + n_a, \quad n \in [1, N]. \tag{5}$$

After some modifications, we have

$$m_n(x) + r_n(x) = \frac{s(x^s) + e_h(m_n(x)) + \theta_n + n_a - \varepsilon \cdot r_n(x)}{1 - \varepsilon}, \quad n \in [1, N]. \tag{6}$$

Considering the linear factor ε of a high-quality AC, which is nothing else but the error committed on evaluating its focal length, is usually small with $|\varepsilon|<0.1\%$, *e.g.* $\varepsilon \approx \pm 2\mu rad/10000\mu rad = \pm 0.02\%$ in Fig. 1(c), and the reference-beam AC reading $r_n(x)$ is within ± 5 μrad, the term $\varepsilon \cdot r_n(x)$ is within ± 5 nrad which is negligible while the noise n_a is at 100 nrad RMS level.

$$m_n(x) + r_n(x) \approx \frac{s(x^s) + e_h(m_n(x)) + \theta_n + n_a}{1 - \varepsilon}, \quad n \in [1, N]. \tag{7}$$

That is to say, for any n and x, there are infinite combinations of ε with $s(x^s) + e_h(m_n(x)) + \theta_n$ that can match the measured value $m_n(x) + r_n(x)$. Since this ambiguity is a linear factor on angles and the X-ray mirror is usually in a concave or convex shape, this linear slope ambiguity is also called as curvature ambiguity. To regularize this ill-posed problem, we regularize the linear factor $\varepsilon = 0$, then the solution of SUT slope $s(x^s)$, the high-order instrument error $e_h(m)$, and the pitch θ_n will be unique. Of course, by doing so, we will suffer from a curvature error in the X-ray mirror measurement, close to $\varepsilon<0.1\%$. With this very small error, this regularization is acceptable for X-ray mirror shape measurement.

Putting both regularization together, Eq. (4) becomes the following constrained linear least-squares optimization problem.

$$\begin{aligned} \min_{\boldsymbol{c},\boldsymbol{f},\boldsymbol{\theta}} \quad & \sum_{n=1}^{N} \sum_{x} \left(m_n(x) + r_n(x) - \boldsymbol{B}(x + d \cdot \theta_n)\boldsymbol{c}^\top - \boldsymbol{E}(m_n(x))\boldsymbol{f}^\top - \theta_n \right)^2 \\ \text{s.t.} \quad & \theta_1 = 0, \\ & \boldsymbol{E}(0)\boldsymbol{f}^\top = 0, \\ & (\boldsymbol{H}^\top \boldsymbol{H})^{-1} \boldsymbol{H}^\top \boldsymbol{E}(\boldsymbol{m})\boldsymbol{f}^\top = 0, \end{aligned} \tag{8}$$

Optics EXPRESS

where the vector $\boldsymbol{H} = \boldsymbol{m}^{\top}$. This constrained linear least-squares problem illustrated in Eq. (8) can be solved by using the MATLAB function *lsqlin(·)* with the "active-set" algorithm.

The angular periodic ambiguity with uniform pitch steps. If a uniform pitch step $\Delta\theta$ is used, with the previously constrain $\theta_1 = 0$, the nth pitch angle is $\theta_n = (n-1)\cdot\Delta\theta$. If we consider there is a periodic function $p(s) = p(s+P)$ with period of $P = \Delta\theta/k,\ k \in \mathbb{N}$, we have

$$p(s) = p(s+P) = p(s+(n-1)\cdot k\cdot P) = p(s+(n-1)\cdot\Delta\theta) = p(s+\theta_n). \tag{9}$$

Considering $r_n(x)$ and $e(m_n(x))$ are commonly much smaller than $m_n(x)$ when measuring curved mirrors, we have the following approximation

$$p(s(x^s)+\theta_n) = p(m_n(x)) + r_n(x) - e(m_n(x)) \approx p(m_n(x)). \tag{10}$$

Applying Eq. (9) and Eq. (10) to Eq. (1), we get

$$\begin{aligned} m_n(x) + r_n(x) &= s(x^s) + e(m_n(x)) + \theta_n + n_a \\ &\approx s(x^s) - p(s(x^s)) + p(m_n(x)) + e(m_n(x)) + \theta_n + n_a \\ &\approx s'(x^s) + e'(m_n(x)) + \theta_n + n_a. \end{aligned} \tag{11}$$

where $s'(x^s) = s(x^s) - p(s(x^s))$ and $e'(m_n(x)) = e(m_n(x)) + p(m_n(x))$. Since the periodic function $p(s)$ is not unique and actually has infinite possibilities, there are ambiguities in the solutions of SUT slope $s(x^s)$ and instrument error $e(m_n(x))$ from the same measured dataset $m_n(x)$ and $r_n(x)$.

To avoid this ambiguity, similar to the solutions in the self-calibration stitching interferometry [24,25], we can introduce random variations to the pitch angles in data acquisition to "break" their periodicity. We demonstrate its effectiveness with a simulation result shown in Fig. 3. Weighted cosine fluctuations with a period around 322 μrad are used to simulate the regional middle-frequency waviness of the instrument error. The angular measurement noise is set as 100 nrad RMS. The global "angular tilt" is not estimated from this multi-pitch approach as mentioned above. By maintaining the same averaged pitch step $\overline{\Delta\theta} = 200$ μrad and the spacing of slope B-spline control point $d_{cp} = 40$ μrad, we compare the results of using different standard deviations of the pitch step randomization $\sigma_{\Delta\theta} = 0$, 1, and 30 μrad. This clearly demonstrates that the periodic error can be significantly suppressed if enough random variations exist in pitch angles.

Although the pitch angle steps are typically performed with certain intrinsic randomization at the sub-μrad to μrad RMS level due to the mechanical limitation, we want to highlight that an extra randomization is still necessary. As compared in the Power Spectral Density (PSD) curves of the reconstructed instrument errors in Fig. 4, even though $\sigma_\theta = 1\mu$rad pitch step variations exist, the two error peaks of the angular period ($P = \Delta\theta/k,\ k \in \mathbb{N}$) at 200 μrad ($k = 1$) and 100 μrad (k=2) still appear, while there is no obvious such peaks with $\sigma_\theta = 30$ μrad pitch step variations.

2.3. Density of slope sampling and control points

Apart from the above ambiguities, some restrictions for the slope sampling and control points spacing need to be noted as well. Based on the Nyquist-Shannon sampling theorem, to properly reconstruct the instrument error with uniform cubic B-splines, the slope sampling frequency f_s should be at least two times higher than the highest frequency $f_h = 1/P_h$ component to reconstruct, *i.e.* $f_s \geq 2f_h$. In practice, considering the angular measurement noise, the samplings should be denser. The control points of B-splines should have a proper density to represent the highest frequency but without over-fitting artifacts. Usually, we set the spacing of control point d_{cp} as one third of the smallest period to reconstruct, *i.e.* $d_{cp} = P_h/3$.

For instance, we simulate an instrument error with two periods, $P_1 = 322$ μrad and $P_2 = 13.33$ μrad, as shown with the black curve in Fig. 5(a). If the slope samplings period $P_s = 3.33$ μrad

Optics EXPRESS

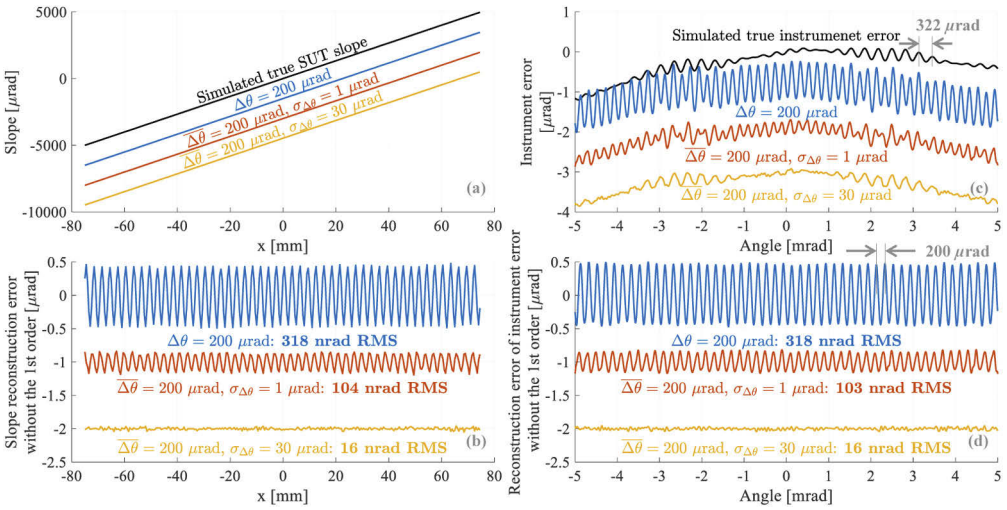

Fig. 3. Enough random variations on the pitch steps can suppress the periodic errors on both the reconstructed SUT slope and the reconstructed instrument error due to the angular periodic ambiguity. (a) the SUT slope reconstruction under different conditions, (b) the reconstruction error of the SUT slope without the linear term, (c) the instrument error reconstruction under different conditions, and (d) the reconstruction error of the instrument error without the linear term.

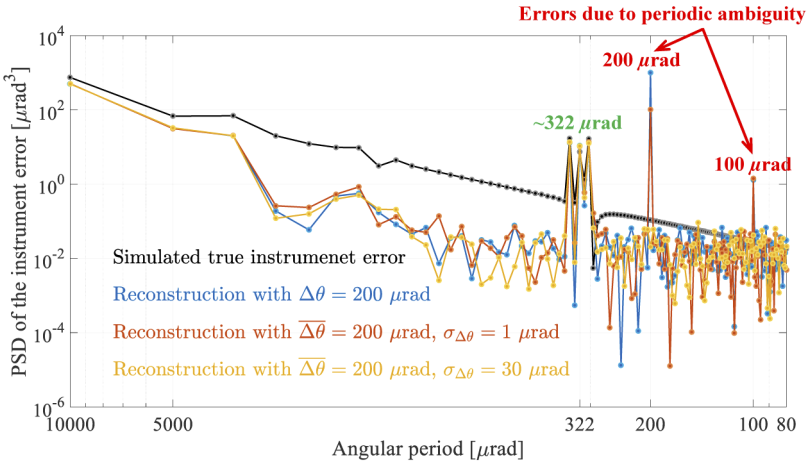

Fig. 4. The PSD plots of the instrument error reconstructions of Fig. 3(c) also indicate the error from periodic ambiguity can be reduced by applying enough randomization on pitch steps.

along the x scanning on a spherical cylindrical SUT, the nonuniform pitch step with average step size of $\overline{\Delta\theta} = 200$ μrad, and the spacing of slope control points d_{cp} is set as $d_{cp} = P_2/3 \approx 4.44$ μrad, both variations with periods of P_1 and P_2 are reconstructed as shown in Fig. 5.

If the slope samplings are not dense enough to represent the highest-frequency f_h fluctuation of the instrument error, it is impossible to retrieve the finest periodic variations in the instrument error, but we still can reconstruct a lower-frequency trend of the instrument error with a suitable d_{cp} selection. Using the previous example, if we used an x-step providing 66.67 μrad/step along the x scan on SUT, and the other conditions maintain the same, *i.e.* $\overline{\Delta\theta} = 200$ μrad and the slope

Optics EXPRESS

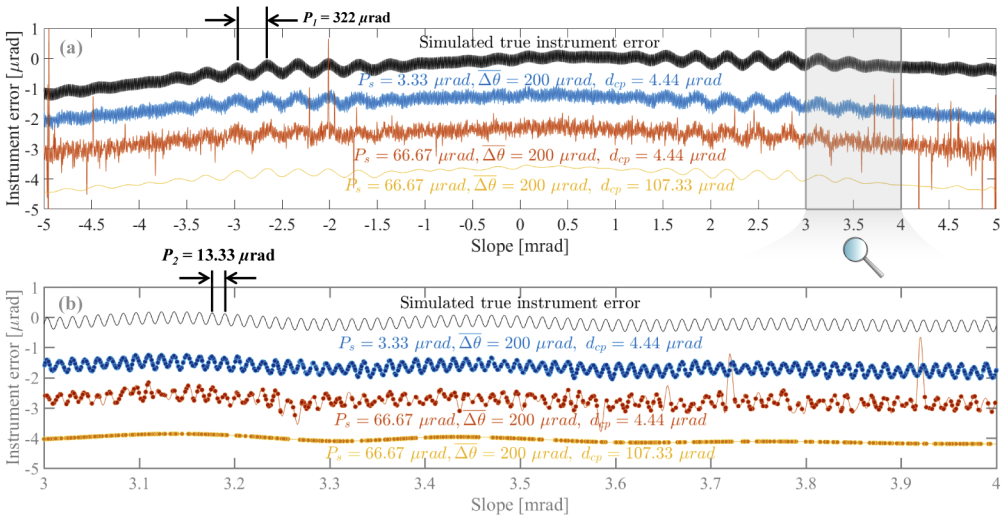

Fig. 5. Reconstruction of the instrument error with two major periods, P_1 = 322 μrad and P_2 = 13.33 μrad, under the conditions of different sampling period P_s, the average pitch step $\overline{\Delta\theta}$, and the spacing of control points d_{cp} (a) within 10 mrad range, and (b) a close view from 3 mrad to 4 mrad (The dots stand for the slope samplings.) shows that large reconstruction errors occurs at periods with insufficient sampling points.

control point spacing d_{cp} = 4.44 μrad, we will then get large artificial errors due to the insufficient samplings on the slope for some periods as illustrated by the red curves in Fig. 5. However, despite that the finest period P_2 = 13.33 μrad are not reconstructed, the lower-frequency trend and P_1 = 322 μrad periodic variations of the instrument error can be reconstructed by setting the spacing of the control points as $d_{cp} = P_1/3$ = 107.33 μrad (the yellow curve) in Fig. 5.

3. Experimental determination of the instrument error

In order to validate our model and method, we have performed a series of experiment by using the NSLS-II NSP instrument [11] with the multi-pitch self-calibration technique. The SUT used in the experiment is a 150-mm-long spherical cylindrical mirror fabricated by JTEC Corp. with a tangential radius of curvature $R \approx$ 15 m and a 10 mrad total slope range. The measured residual slope error derived from the stitching height data from the manufacturer is about 70 nrad RMS. This is a perfect match for the self-calibration study of the 10-mrad-measuring-range Möller-Wedel Elcomat 3000 AC. The mirror is placed on a motorized pitch stage, and the SUT is about 10 mm under the sample-beam AC with a 2.5-mm-diameter pinhole.

3.1. Repeatability of the instrument error determination in two continuous sets of measurement

The first two continuous sets of multi-pitch measurement are scanned with the SUT in A2B orientation (Here the "A2B" orientation means that the SUT is measured from its one end "A" to the other end "B". By physically rotating the mirror 180° we will have the SUT in the opposite orientation named "B2A".). The raw slope data of these two sets of measurement are shown in Figs. 6(a) and 6(b). The temperature variations shown in Fig. 6(c) are less than 0.05 °C PV for both scans. The active pitch range is about 10 mrad and the average pitch step $\overline{\Delta\theta}$ = 100 μrad. In total, 101 pitch angles are scanned to provide the redundant slope data. At each pitch angle, the SUT is scanned in 147 mm with a sampling step Δx = 1 mm. To reduce the influence from the drift, "forward and backward" scans are performed and averaged as the result of each x scan.

Optics EXPRESS

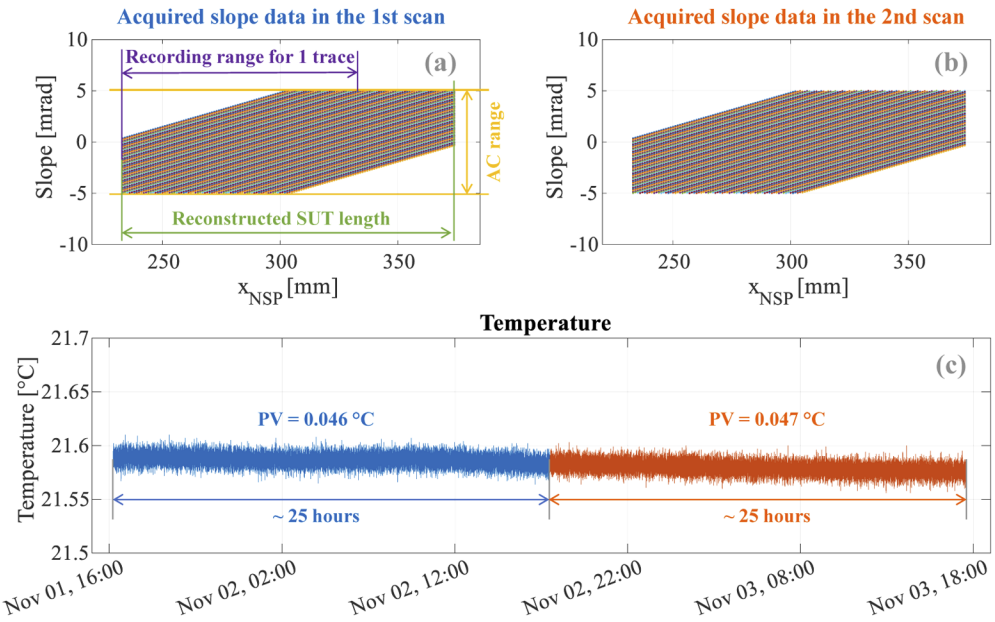

Fig. 6. Two continuous multi-pitch self-calibration measurements in 101 pitch angles with $\overline{\Delta\theta}$ = 100 μrad are performed with slope data acquisition (a) from 01 Nov, 2019 to 02 Nov, 2019 and (b) from 02 Nov, 2019 to 03 Nov, 2019. The temperature (c) measured during these two scans are stabled with 0.046 °C PV and 0.047 °C PV variation, respectively.

In the reconstruction, the spacing of the slope control points is set as d_{cp} = 100 μrad to reconstruct the low-frequency instrument error only. The reconstructed SUT slope errors, instrument errors, and the pitch angles are plotted in blue and orange curves in Figs. 7(a), 7(c), and 7(e).

These two sets of scans are repeatable. As shown in Fig. 7(b), the difference of two reconstructed SUT slope errors is 12 nrad RMS, and the discrepancy of the reconstructed instrument error is 12 nrad RMS in Fig. 7(d). The differences between the estimated pitch angles and the pitch-beam AC measured angles are shown in Fig. 7(f).

3.2. *Reproducibility of the instrument error determination*

The SUT was then measured in A2B orientation with 51 pitch angles over 10 mrad with $\overline{\Delta\theta}$ = 200 μrad, and then the SUT was rotated 180° to take B2A 51-pitch scans with $\overline{\Delta\theta}$ = 200 μrad. The resultant SUT slope errors and instrument errors are shown in Figs. 8(a) and 8(c).

If we take the average of the two previous $\overline{\Delta\theta}$ = 100 μrad scans in Fig. 7 as our reference in the following comparison, the discrepancies of $\overline{\Delta\theta}$ = 200 μrad A2B and B2A scans from the reference are only 20 nrad RMS and 53 nrad RMS for the SUT slope and 20 nrad RMS and 15 nrad RMS for the instrument error as shown in Figs. 8(b) and 8(d), respectively. From the PSD of the reconstructed instrument errors shown in Fig. 8(e), we can see the main period of the low-frequency fluctuation in the instrument error is about 322.6 μrad.

To reconstruct high-frequency fluctuations in the instrument error, small steps are preferred to avoid the issue of insufficient samplings. For example, another A2B multi-pitch scan with Δx = 0.1 mm and $\overline{\Delta\theta}$ = 20 μrad are performed in a pitch range of [-0.5, 0.5] mrad. The resultant instrument error is illustrated in Fig. 9(a) and enlarged in Fig. 9(b), in which the reference low-frequency instrument error of Fig. 8 is also plotted to show the self-consistency in trend.

Optics EXPRESS

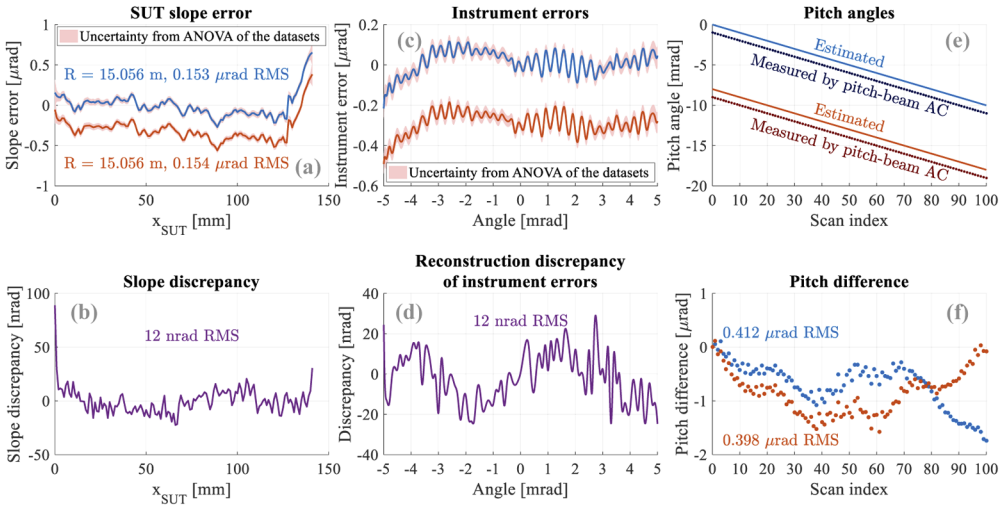

Fig. 7. Two multi-pitch self-calibration scans in 101 pitch angles with $\overline{\Delta\theta} = 100$ μrad (blue: the 1st scan, red: the 2nd scan). (a) Reconstructed SUT slope errors with the same sphere removed (the red regions indicating the $\pm 2\sigma$ uncertainty range obtained by analysis of the variance (ANOVA) of the datasets), (b) the discrepancy of two SUT slope reconstruction, (c) the reconstructed instrument error of the sample-beam AC (the red regions indicating the $\pm 2\sigma$ uncertainty range), (d) the discrepancy of two reconstruction of instrument errors, (e) the measured pitch angles by pitch-beam AC and the estimated pitch angles, and (f) the differences between the estimations and measurements. Some curves are vertically shifted for better visual comparison.

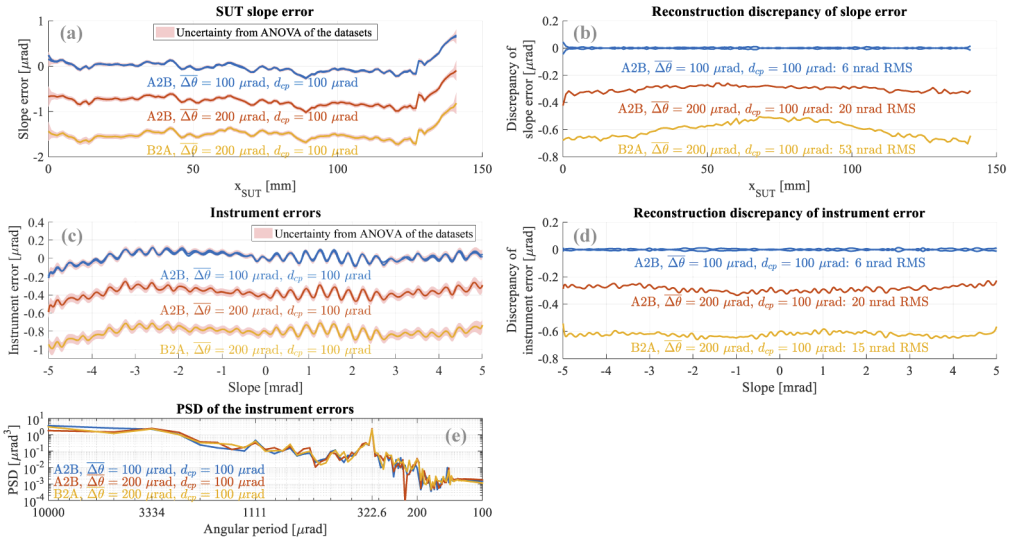

Fig. 8. Taking the 101-pitch A2B scans with $\overline{\Delta\theta} = 100$ μrad as the reference, 51-pitch A2B and B2A scans with $\overline{\Delta\theta} = 200$ μrad are compared. (a) Reconstructed SUT slope (the red regions indicating the $\pm 2\sigma$ uncertainty range), (b) their discrepancies from the reference SUT slopes, (c) reconstructed instrument errors (the red regions indicating the $\pm 2\sigma$ uncertainty range), (d) the reconstruction discrepancy of instrument errors from the reference results, and (e) the PSD of the instrument errors.

Optics EXPRESS

Figure 9(c) displays the PSDs of the three instrument errors, which indicates the period of the high-frequency fluctuations of the sample-beam AC is about 13.33 μrad.

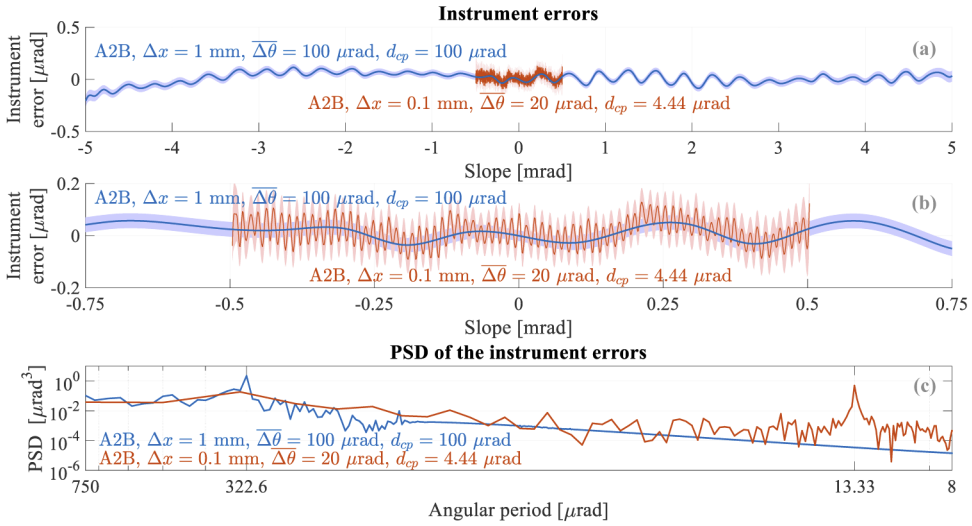

Fig. 9. The 20-μrad-step multi-pitch scans can reconstruct the high-frequency instrument error. (a) Comparison of the reconstructed instrument errors with $\pm 2\sigma$ uncertainty regions indicated, (b) is a zoom-in view of (a), and (c) the PSD of the instrument errors.

3.3. *Effective compensation with the estimated instrument error*

To check the effectiveness of applying the reconstructed instrument error from Fig. 8 for slope error compensation, another two sets of A2B and B2A usual scans are repeated 50 times with no active pitch. For a clear comparison, their averaged SUT slope residuals before and after the instrument error compensation are shown in Fig. 10(a). The result shows effective compensation of the "waviness" in green ovals for both scans. If we take the SUT slope error of the previous 101-pitch A2B scan as the reference for comparison, the discrepancies from the reference and the slope compensation amount according to the instrument error "look-up" curve are plotted in Fig. 10(b). Since the instrument error is related on the angle, not x-position, the "waviness" in green ovals on A2B and B2A slope errors locate at different x-positions.

Optics EXPRESS

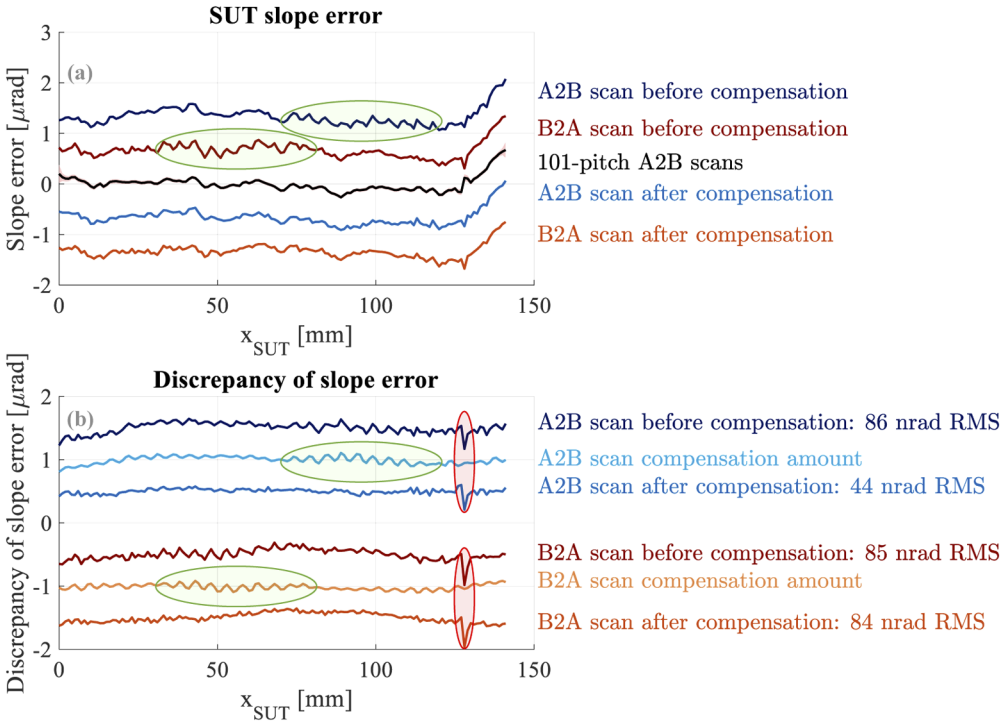

Fig. 10. The A2B and B2A normal scans are compensated by the reconstructed instrument errors. (a) SUT slope error before and after compensation, and (b) the compensation amount and the discrepancies of the slope errors before and after compensation with respect to the 101-pitch A2B scans.

4. Discussion

As demonstrated above in both simulation and experiment, the multi-pitch self-calibration technique applied to the NSP instrument can reconstruct the SUT slope, systematic instrument error, and the introduced pitch angles at the same time. Here we would like to address some features when using multi-pitch method with an NSP measurement system.

This technique is useful to decouple the mirror surface slope and the NSP systematic error from the acquired redundant measurement data. The experimental results indicates the reconstruction of the SUT slope and NSP instrument error is repeatable and reproducible. In addition, the instrument error extracted from the multi-pitch measurement can be used to correct single-pitch scans as was demonstrated in section 3.3. Furthermore, the multi-pitch method allows slope stitching ability to extend the measuring range of the NSP instrument.

It is important to emphasize that the temperature change induces angle drifts between the SUT and the measuring equipment. During a multi-pitch scan, its main effect, on the short term, is to distort the individual profiles. On the long term it also produces a drift of the average slope value of one profile with respect to others. Since pitch angle θ_n does not need to be measured and is a parameter of the fit, this drift is taken into account in the actual θ_n value. Therefore, stability should be only assured on the acquisition time of one profile which is in our case 5.5 mK over 15 minutes.

We would also want to highlight that equidistant pitches introduce a periodic error despite that the slope sampling points are not equidistant. Random variations on pitch angles can be

Optics EXPRESS

employed to depress this periodic error. Moreover, the slope sampling points should be dense enough in order to fully reconstruct the instrument error.

In addition to the above-mentioned merits of applying the multi-pitch method to the NSP instrument, we would also like to discuss some of the limitations and concerns of this approach.

The linear term of the instrument error cannot be recovered with this method, but can be calibrated separately by using a curved mirror with a known curvature. This is a general issue of all slope measuring instruments.

The distance d between the pitch rotation axis and the mirror surface needs to be determined before taking the multi-pitch calculation. Owing to this distance d, the sampling points on the SUT are not exactly at the same locations for different tilts. It will be better if the pitch rotation axis can be placed close to the SUT to reduce the lateral shift of the sampling positions. The error of this distance is one of the error sources of the multi-pitch self-calibration method.

Moreover, due to the lateral shift caused by the distance d, some of the local high-frequency spikes on the SUT may not be sampled in the scans at different pitch angles. The model-based estimation algorithm (B-spline in our case) will treat these "flickering" signals as the measurement noise. As a result, these surface details may not be resolved as illustrated in the red ovals in Fig. 10(b). At certain level, there is always a question mark for a model-based fitting method to judge whether it is a signal or noise.

To get the high-frequency instrument errors, the stability of the roll axes needs to be considered, as the angle readings in the other direction of the sample-beam AC may have similar high-frequency errors. A possible improvement on this is to make multi-pitch-and-roll self-calibration scans to get the two-dimensional instrument error map like in Ref. [26].

5. Conclusion

We present the application of multi-pitch self-calibration method on the NSLS-II NSP instrument for X-ray mirror nanoradian slope metrology. During its x-scan and pitch-scan, the NSP has a distance-fixed sample-beam AC. It is consequently an ideal application scenario for the multi-pitch method. Ambiguities of the multi-pitch method are addressed and several practical solutions and regularization are proposed to solve this ill-posed problem. In our experiment with a 10-mrad total slope spherical mirror, the SUT slope and the low-frequency instrument errors (period larger than 300 μrad) can be repeatably reconstructed with different pitch settings and mirror orientations. This multi-pitch self-calibration method is a good approach to measure mirrors whose total slope is larger than the measuring range of the sample-beam AC or the moving optical head.

Funding

Office of Science (DE-SC0012704); Ministerio de Ciencia, Innovación y Universidades (RTI2018-097107-B-C32).

Acknowledgments

The authors want to thank Shinan Qian for the establish and development of the NSP instrument, and Dennis Kuhne from the Research & Development Group of NSLS-II for the mechanical machining. This research used resources of the National Synchrotron Light Source II, a U.S. Department of Energy (DOE) Office of Science User Facility operated for the DOE Office of Science by Brookhaven National Laboratory under Contract No. DE-SC0012704.

Disclosures

The authors declare that there are no conflicts of interest related to this article.

Optics EXPRESS

References

1. R. J. Bean, A. Aquila, L. Samoylova, and A. P. Mancuso, "Design of the mirror optical systems for coherent diffractive imaging at the SPB/SFX instrument of the european XFEL," J. Opt. **18**(7), 074011 (2016).
2. P. Z. Takacs, S. nan Qian, and J. Colbert, "Design Of A Long Trace Surface Profiler," *Metrology: Figure and Finish*, vol. 0749 B. E. Truax, ed., International Society for Optics and Photonics (SPIE, 1987), pp. 59–64.
3. S. Qian, W. Jark, and P. Z. Takacs, "The penta-prism LTP: A long-trace-profiler with stationary optical head and moving penta prism," Rev. Sci. Instrum. **66**(3), 2562–2569 (1995).
4. M. Thomasset, S. Brochet, and F. Polack, "Latest metrology results with the SOLEIL synchrotron LTP," *Advances in Metrology for X-Ray and EUV Optics*, vol. 5921 L. Assoufid, P. Z. Takacs, and J. S. Taylor, eds., International Society for Optics and Photonics (SPIE, 2005), pp. 12–20.
5. A. Rommeveaux, O. Hignette, and C. Morawe, "Mirror metrology and bender characterization at ESRF," in *Advances in Metrology for X-Ray and EUV Optics*, vol. 5921 L. Assoufid, P. Z. Takacs, and J. S. Taylor, eds., International Society for Optics and Photonics (SPIE, 2005), pp. 167–174.
6. F. Siewert, T. Noll, T. Schlegel, T. Zeschke, and H. Lammert, "The nanometer optical component measuring machine: a new sub-nm topography measuring device for X-ray optics at BESSY," AIP Conf. Proc. **705**, 847–850 (2004).
7. S. Alcock, K. Sawhney, S. Scott, U. Pedersen, R. Walton, F. Siewert, T. Zeschke, F. Senf, T. Noll, and H. Lammert, "The Diamond-NOM: A non-contact profiler capable of characterizing optical figure error with sub-nanometre repeatability," Nucl. Instrum. Methods Phys. Res., Sect. A **616**(2-3), 224–228 (2010).
8. V. V. Yashchuk, S. Barber, E. E. Domning, J. L. Kirschman, G. Y. Morrison, B. V. Smith, F. Siewert, T. Zeschke, R. Geckeler, and A. Just, "Sub-microradian surface slope metrology with the als developmental long trace profiler," Nucl. Instrum. Methods Phys. Res., Sect. A **616**(2-3), 212–223 (2010).
9. J. Nicolas and J. C. Martínez, "Characterization of the error budget of Alba-NOM," Nucl. Instrum. Methods Phys. Res., Sect. A **710**, 24–30 (2013).
10. S. Qian, L. Wayne, and M. Idir, "Nano-accuracy measurements and the surface profiler by use of monolithic hollow penta-prism for precision mirror testing," Nucl. Instrum. Methods Phys. Res., Sect. A **759**, 36–43 (2014).
11. S. Qian and M. Idir, "Innovative nano-accuracy surface profiler for sub-50 nrad rms mirror test," *8th International Symposium on Advanced Optical Manufacturing and Testing Technologies: Subnanometer Accuracy Measurement for Synchrotron Optics and X-Ray Optics*, vol. 9687 S. Qian, M. Idir, D. Cocco, T. Xiao, and K. Yamauchi, eds., International Society for Optics and Photonics (SPIE, 2016), pp. 81–90.
12. I. Lacey, K. Anderson, G. P. Centers, R. D. Geckeler, G. S. Gevorkyan, J. Grossiord, A. Just, T. Nicolot, B. V. Smith, and V. V. Yashchuk, "The ALS OSMS: Optical Surface Measuring System for high accuracy two-dimensional slope metrology with state-of-the-art x-ray mirrors," in *Advances in X-Ray/EUV Optics and Components XIII*, vol. 10760 S. Goto, C. Morawe, and A. M. Khounsary, eds., International Society for Optics and Photonics SPIE, 2018), pp. 11–30.
13. F. Yang, M. Li, Q. Cai, W. Sheng, P. Liu, and X. Zhang, "New surface slope profiler with sub-millimeter spatial resolution," in *Advances in Metrology for X-Ray and EUV Optics VIII*, vol. 11109 L. Assoufid, H. Ohashi, and A. Asundi, eds., International Society for Optics and Photonics (SPIE, 2019), pp. 166–171.
14. R. D. Geckeler and A. Just, "Distance-dependent influences on angle metrology with autocollimators in deflectometry," in *Advances in X-Ray/EUV Optics and Components III*, vol. 7077 A. M. Khounsary, C. Morawe, and S. Goto, eds., International Society for Optics and Photonics (SPIE, 2008), pp. 85–96.
15. R. D. Geckeler, P. Křen, A. Just, M. Schumann, M. Krause, I. Lacey, and V. V. Yashchuk, "Environmental influences on autocollimator-based angle and form metrology," Rev. Sci. Instrum. **90**(2), 021705 (2019).
16. I. Lacey, K. Anderson, J. Dickert, R. D. Geckeler, A. Just, F. Siewert, B. V. Smith, and V. V. Yashchuk, "Transfer of autocollimator calibration for use with scanning gantry profilometers for accurate determination of surface slope and curvature of state-of-the-art x-ray mirrors," in *Advances in Metrology for X-Ray and EUV Optics VIII*, vol. 11109 L. Assoufid, H. Ohashi, and A. Asundi, eds., International Society for Optics and Photonics (SPIE, 2019), pp. 33–48.
17. E. Debler and K. Zander, "Ebenheitsmessung an optischen planflächen mit autokollimationsfernrohr und pentagonprisma," PTB Mitteilungen Forschen + Prüfen, Amts und Mitteilungsblatt der Physikalisch Technischen Bundesanstalt, Braunschweig und Berlin **89**, 339–349 (1980).
18. F. Siewert, J. Buchheim, and T. Zeschke, "Characterization and calibration of 2nd generation slope measuring profiler," Nucl. Instrum. Methods Phys. Res., Sect. A **616**(2-3), 119–127 (2010).
19. T. Yandayan, "Recent developments in nanoradian-angle metrology," in *Advances in Metrology for X-Ray and EUV Optics VII*, vol. 10385 L. Assoufid, H. Ohashi, and A. K. Asundi, eds., International Society for Optics and Photonics (SPIE, 2017), pp. 58–71.
20. F. Polack, M. Thomasset, S. Brochet, and A. Rommeveaux, "An LTP stitching procedure with compensation of instrument errors: Comparison of soleil and esrf results on strongly curved mirrors," Nucl. Instrum. Methods Phys. Res., Sect. A **616**(2-3), 207–211 (2010).
21. F. Polack and M. Thomasset, "determination and compensation of the reference surface from redundant sets of surface measurements," Nucl. Instrum. Methods Phys. Res., Sect. A **710**, 67–71 (2013).
22. J. Nicolas and J. Campos, "Error compensation for the calibration of mechanical mirror benders," in Advances in X-Ray/EUV Optics and Components VIII, vol. 8848 A. Khounsary, S. Goto, and C. Morawe, eds., International Society for Optics and Photonics (SPIE, 2013), pp. 144–151.

Optics EXPRESS

23. J. Nicolas, P. Pedreira, I. Šics, C. Ramírez, and J. Campos, "Nanometer accuracy with continuous scans at the ALBA-NOM," in *Advances in Metrology for X-Ray and EUV Optics VI*, vol. 9962 L. Assoufid, H. Ohashi, and A. K. Asundi, eds., International Society for Optics and Photonics (SPIE, 2016), pp. 14–21.
24. J. Nicolas, M. L. Ng, P. Pedreira, J. Campos, and D. Cocco, "Completeness condition for unambiguous profile reconstruction by sub-aperture stitching," Opt. Express **26**(21), 27212–27220 (2018).
25. L. Huang, T. Wang, J. Nicolas, A. Vivo, F. Polack, M. Thomasset, C. Zuo, K. Tayabaly, D. W. Kim, and M. Idir, "Two-dimensional stitching interferometry for self-calibration of high-order additive systematic errors," Opt. Express **27**(19), 26940–26956 (2019).
26. V. Heikkinen, V. Byman, M. Shpak, R. Geckeler, A. Just, M. Krause, M. Schumann, and A. Lassila, "High-accuracy autocollimator calibration by interferometric 2D angle generator," in *Advances in Metrology for X-Ray and EUV Optics VIII*, vol. 11109 L. Assoufid, H. Ohashi, and A. Asundi, eds., International Society for Optics and Photonics (SPIE, 2019), pp. 15–24.